Microglial refinement of spinal cord sensory circuitry regulates normal maturation of dynamic touch

Yajing Xu, Stephanie C. Koch, Alexander Chamessian, Qianru He, Mayya Sundukova, Paul Heppenstall, RuRong Ji, Maria Fitzgerald, Simon Beggs*

Affiliations

Neuroscience, Physiology and Pharmacology, UCL, London, UK

Yajing Xu, Stephanie C. Koch, Maria Fitzgerald and Simon Beggs

UCL Great Ormond Street Institute of Child Health, London, UK

Simon Beggs

Center for Translational Pain Medicine, Department of Anesthesiology[2], Cell Biology[3], Duke University Medical Centre, Duke University, Durham, NC, USA

Alexander Chamessian[2], Qianru He[3], RuRong Ji[2,3]

Epigenetics & Neurobiology Unit, European Molecular Biology Laboratory, Rome, Italy

Paul Heppenstall, Mayya Sundukova

Abstract

In the spinal cord dorsal horn, sensory circuits undergo remarkable postnatal reorganisation, including refinement of primary afferent A-fibres in the superficial layers, accompanied by decreased cutaneous sensitivity. Here we show a physiological role of microglia necessary for normal development of dorsal horn sensory circuits and tactile sensitivity. In the absence of microglial engulfment, superfluous A-fibre projections persist, leading to lifelong hypersensitivity to dynamic touch.

Main

The neonatal spinal dorsal horn differs substantially from that in adults and primary afferent input undergoes extensive structural and functional reorganisation over the postnatal period[1,2]. In order to convey an accurate representation of the tactile world, mechanosensitive afferents must preserve somatotopically precise information while forming connections with dorsal horn networks that are distinct from those for nociception. This process is shaped by the sensory environment in early life through activity dependent refinement of connections at all levels of the somatosensory nervous system [1,3,4].

Activity dependent refinement is characterized in the developing dorsal horn by the retraction of low-threshold A-fibre axon terminals from the superficial laminae [3,4] accompanied by a reduction in dorsal horn cell receptive field size and tactile sensitivity [1,5,6] and in behavioural responses to touch [7]. However, the mechanism underlying the remodelling of A-fibre terminals in the dorsal horn is not known. Microglia have been shown to sculpt the sensory neuronal environment within the developing visual system; removing apoptotic cells and phagocytosing synapses and neurites during postnatal refinement [8]. We hypothesised that the disappearance of

A-fibres from superficial laminae in the early postnatal period is driven by microglial pruning, and that disruption of microglial function will impair normal postnatal structural refinement of tactile spinal sensory circuits and sensitivity to touch.

In the developing spinal cord, tactile-encoding A-fibres initially project throughout the dorsoventral extent of the dorsal horn and refine over the first few postnatal weeks to terminate in deeper laminae, segregated from the more superficial terminals of noxious-encoding C-fibres [3]. We confirmed this using a transgenic reporter mouse in which tdTomato is expressed in vesicular glutamate transporter 1 (*Vglut1*) expressing neurons (VGLUT1-tdT), a population of large myelinated sensory neurons with features consistent with Aβ-low threshold mechanoreceptors (LTMRs) [9]. The central axon terminals of these neurons extend into the superficial laminae in the early postnatal period (Fig. 1a), with flame-shaped arbors extending into laminae I-II (white arrowheads in Fig. 1a, enlarged in 1b), but are no longer present in these superficial laminae by P28.

Next, we determined the phagocytic activity of dorsal horn microglia over this period by the presence of phagocytic cups (Fig. 1c,d) and the lysosome associated molecular marker CD68 (Fig. 1c,e). Both measures were elevated during the first postnatal week (Fig. 1d,e) (Phagocytic cups: $F(3, 12)=10.97$, $P=0.0009$, CD68-expressing microglia: $F(3, 12)=16.20$, $P=0.0002$). In parallel, microglial density and their ratio to neurons increased, while apoptotic cell numbers decreased (Fig. S1, S2), suggesting the first postnatal week represents a distinct period of microglial activity.

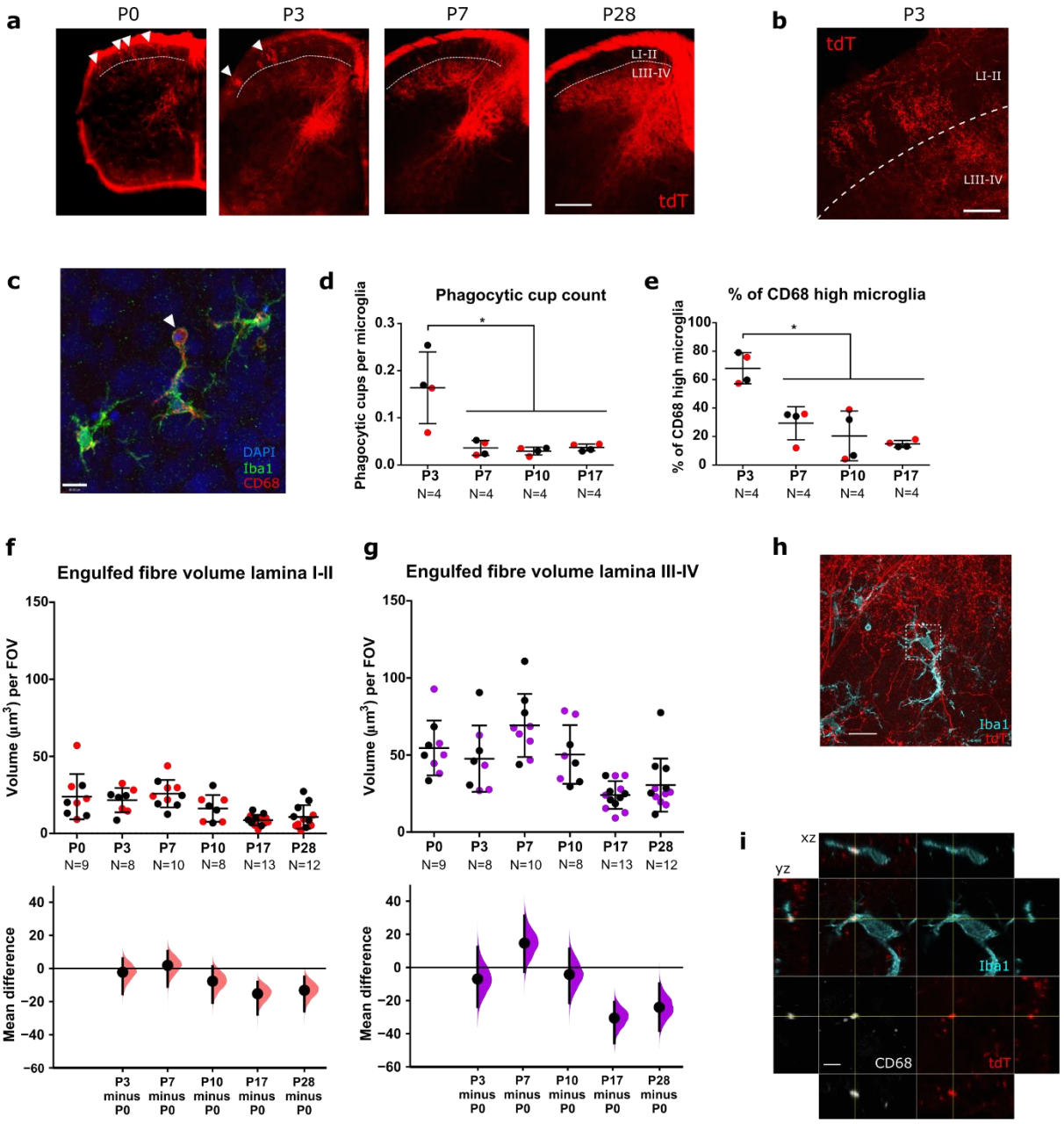

Figure 1. Dorsal horn microglia engulf A-fibres during normal postnatal development

a. Representative images of tdTomato (red) expression across ages. Dashed white line indicates border between lamina II and lamina III, white arrow heads indicate A-fibres in the superficial laminae I-II. Scale bar = 200µm.

b. High magnification of exuberant A-fibre bundles in laminae I-II at P3. Dashed white line indicates border between lamina II and lamina III. Scale bar = 50µm.

c. Representative image of a P3 dorsal horn microglia (Iba1, green) with phagocytic cup (CD68, red). White arrowhead indicate coexpression. DAPI (blue). Scale bar = 10µm.

d. Phagocytic cup count per microglia decreases significantly between P3 and P7, ($P < 0.01$ for all ages compared to P3).

e. The percentage of CD68 high microglia decreases with postnatal age between P3 and P7 ($P < 0.01$ for all ages compared to P3).

f. Microglial phagocytosis of A-fibres in laminae I-II decreases with postnatal age. P3 vs P0: mean difference -2.26 [95% CI -15.46, 6.05]; P7 vs P0: mean difference 1.88 [95% CI -10.94, 10.53]; P10 vs P0: mean difference -7.68 [95% CI -20.66, 1.31]; P17 vs P0: mean difference -15.23 [95% CI -27.73, -8.14]; P28 vs P0: mean difference -13.19 [95% CI -25.85, -5.06].

g. Microglial phagocytosis of A-fibres in laminae III-IV decreases with postnatal age. P3 vs P0: mean difference -6.96 [95% CI -23.80, 12.32]; P7 vs P0: mean difference 14.66 [95% CI -2.57, 31.28]; P10 vs P0: mean difference -4.20 [95% CI -21.40, 11.34]; P17 vs P0: mean difference -30.55 [95% CI -45.67, -20.77]; P28 vs P0: mean difference -24.05 [95% CI -38.23, -9.69]. Field of view (FOV) = 245µm x 65µm.

h. Representative image of microglial A-fibre engulfment in the spinal dorsal horn of P3 VGLUT1-tdt mice, stained for microglia (Iba1, cyan), microglial lysosomes (CD68, white) and endogenously fluorescent A-fibres (tdTomato, red). Scale bar = 20µm. White inset box show location of higher magnification panels in **i**.

i. High magnification image of microglial A-fibre engulfment in **h** stained for microglia (Iba1, cyan), microglial lysosomes (CD68, white) and endogenously fluorescent A-fibres (tdTomato, red). Cross-hairs show position of the xz and yz side-view panels. Scale bar = 5µm.

N-numbers as indicated. Black and red/magenta data points indicate females and males respectively.

We next asked whether the high phagocytic activity of microglia during the first postnatal week is associated with the refinement of neural connectivity in the dorsal horn through the removal of superfluous A-fibre terminals, as labelled by tdTomato fluorescence in VGLUT1-tdT mice. To identify microglia as the cellular mediators in this refinement, engulfment of A-fibres was measured by quantifying tdT fluorescence volume within CD68-positive lysosomes (Fig. 1h,i).

Consistent with the postnatal period of increased microglial phagocytic activity, the volume of engulfed A-fibres was highest during the first postnatal week, reducing by half at P17 (Fig. 1f,g) in laminae I-II, (unpaired mean difference -15.23 [95% CI -27.73, -8.14]) and laminae III-IV (unpaired mean difference -30.55 [95% CI -45.67, -20.77])

Having established that microglia participate in the postnatal removal of afferent A-fibre terminals in the dorsal horn, we sought to determine whether microglial function is necessary for this process to occur normally. The phospholipid scramblase TMEM16F is required for normal microglial phagocytic activity[10]. Therefore to address this question, we generated a conditional knockout (cKO) mouse line in which *Tmem16f* is selectively deleted in a Cre-dependent manner. We then crossed this line to the microglial-selective *Cx3cr1*^{CreER} mouse line to produce a deficit in microglial phagocytosis in a subset of mice[10]. A *R26*$^{LSL\text{-}Ai9}$ reporter line was used to label Cre-expressing neurons and *Thy1*^{eGFP} allele was used to identify A-fibres[11]. The structural, functional and behavioural consequences of microglial phagocytosis was then assessed in adult animals. To control for off-target effects of Cre expression and tamoxifen administration, both cKO and control mice (*Tmem16f*$^{+/+}$ (*Cx3cr1*$^{CreER/+}$*::Tmem16f*$^{fl/fl}$*::R26*$^{LSL\text{-}Ai9}$*::Thy1*^{eGFP} and *Cx3cr1*$^{CreER/+}$*::Tmem16f*$^{+/+}$*::R26*$^{LSL\text{-}Ai9}$*::Thy1*^{eGFP} respectively) received 4-hydroxytamoxifen (4-HT) daily from P1 to P3 and were assessed at 3-4 months old. Specificity of Cre expression was confirmed with *R26*$^{LSL\text{-}Ai9}$ tdT expression.

Postnatal deletion of microglial *Tmem16f* resulted in adults with increased A-fibre terminal occupancy in the superficial dorsal horn, as revealed by both Thy1-eGFP expression and VGLUT1 immunohistochemistry (Fig. S5, S6). As eGFP is expressed in only a small number of sensory neurons, all subsequent quantification was performed using VGLUT1 immunolabelling. Synaptic density of this increased input was quantified using VGLUT1 immunohistochemistry in laminae I-II (Fig 2a upper panels). *Tmem16f* cKO mice had greater primary afferent VGLUT1 synaptic density throughout the dorsal horn than control mice as measured by both total synapse volume and synapse number (Fig 2b) (unpaired mean difference synapse volume:

799.28 [95.00% CI 450.09, 1136.35], synapse number: 533.67 [95.00% CI 356.12, 695.50]). In contrast, local inhibitory VGAT synapse density was unaltered (Fig 2a lower panels, 2c) (unpaired mean difference synapse volume: -168.31 [95.00% CI -562.61, 253.44], synapse number: -159.19 [95.00% CI -416.42, 148.88]). Thus, targeted deletion of microglial *Tmem16f*, and consequent impaired phagocytosis specifically disrupted the normal developmental pruning of excitatory afferent A-fibre projections in the dorsal horn.

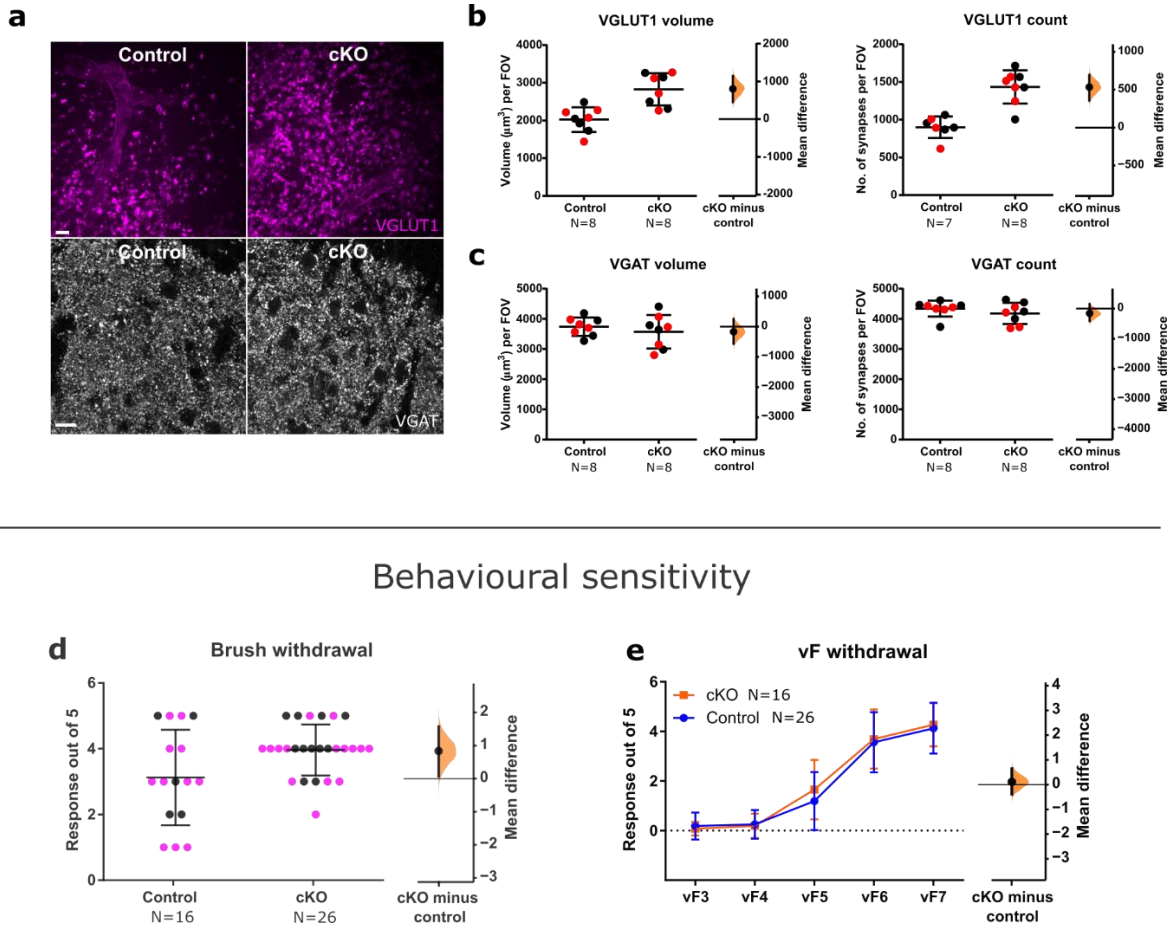

Figure 2. Neonatal *Tmem16f* cKO in microglia disrupts dorsal horn A-fibre terminals and dynamic brush sensitivity.

a. Representative images of VGLUT1 and VGAT puncta from the dorsal horn of *Tmem16f* control and cKO animals. Field of view (FOV) = 94µm x 94µm (VGLUT1), 96µm x 96µm (VGAT). Scale bar = 10µm.

b. VGLUT1 volume and count were both increased in *Tmem16f* cKO animals compared to controls. Control vs cKO volume: mean difference 799.28 [95.00% CI 450.09, 1136.35]; control vs cKO count: mean difference 533.67 [95.00% CI 356.12, 695.50].

c. VGAT volume and count were not significantly different between *Tmem16f* cKO animals and controls. Control vs cKO volume: mean difference -168.3105 [95.00% CI -562.61, 253.44]; control vs cKO count: mean difference -159.19 [95.00% CI -416.42, 148.88].

d. Brush withdrawal response for *Tmem16f* cKO animals are higher than control animals, mean difference 0.83 [95% CI 0.072, 1.57].

e. vF withdrawal response did not differ between *Tmem16f* cKO and control animals, mean difference 0.12 [95% CI -0.39, 0.65].

N-numbers as indicated. Black and magenta/red data points indicate females and males respectively.

We reasoned that the reduced A-fibre pruning as a consequence of impaired neonatal microglial phagocytosis in *Tmem16f* cKO mice would alter behavioural sensitivity to hindpaw tactile stimulation. The hindlimb withdrawal reflex was measured in response to brushing of the plantar surface of the paw. *Tmem16f* cKO mice showed a greater number of withdrawals in response to dynamic brushing than controls (unpaired mean difference 0.83 [95% CI 0.072, 1.57]), but not to vF stimulation (Fig. 2d, e, S4). *Tmem16f* cKO animals therefore displayed cutaneous hypersensitivity specifically towards dynamic low-threshold tactile stimulation.

We hypothesised that excessive A-fibre presence in dorsal horn might lead to increased dorsal horn activity which could underlie the behavioural hypersensitivity. To test this, we used *in vivo* single unit extracellular recordings in the dorsal horn of anaesthetised *Tmem16f* cKO and control mice. We recorded from adapting wide dynamic range neurons (WDR) in the deep dorsal horn, which according to the criteria by Lee et al. 2019 [12] are presumed to be excitatory neurons (Fig. 3e).

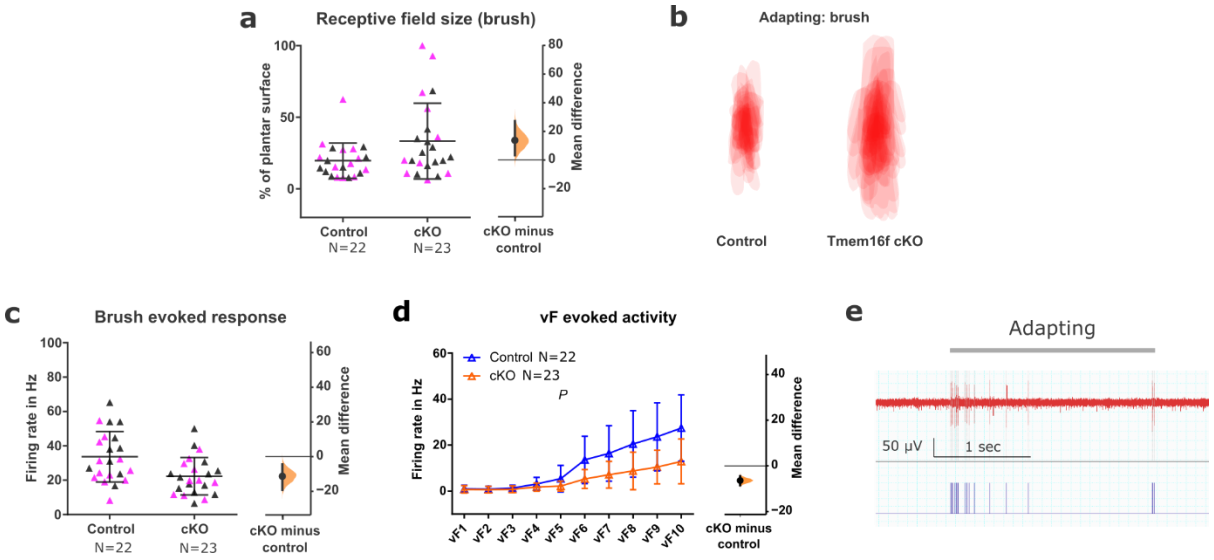

Figure 3. Neonatal *Tmem16f* deletion in microglia decreases peripherally evoked activity, but increases brush-sensitive receptive field area

a. Brush receptive field area of spinal WDR neurons was increased in *Tmem16f* cKO adult animals, mean difference 13.7 [95.00% CI 3.3, 27.2].

b. Overlay of individual brush-sensitive dorsal horn receptive fields plotted in **a.**

c. Brush evoked response of WDR spinal neurons was decreased in *Tmem16f* cKO adult animals, mean difference -11.4 [95% CI -19.2, -4.5].

d. vF evoked static touch activity was decreased *Tmem16f* cKO, mean difference -6.4 [95% CI -8.5, -4.5].

e. Representative firing traces of an adapting cell (R = 0.18) with raster plots underneath. Grey bar above the traces indicates vF stimulus duration.

N-numbers as indicated. Black and magenta data points indicate females and males respectively.

We then quantified their response to 1) dynamic innocuous tactile stimuli (brush), and 2) static von Frey hair (vF) stimuli applied to the plantar hindpaw as well as mapped dynamic touch-sensitive receptive field areas on the plantar hindpaw. We reasoned that excessive A-fibre presence in the dorsal horn would increase their spatial connectivity with postsynaptic neurons, leading to larger dorsal horn receptive field areas. Consistent with a reduction in central A-fibre refinement, mean brush receptive field sizes were increased by almost 50% (unpaired mean difference 13.7 [95.00% CI

3.3, 27.2]), with a notable subpopulation of cKO neurons expanding their receptive fields to cover the entire, or majority of the plantar surface (Fig. 3a, b). The expansion of receptive field area was accompanied by a reduced number of spikes in response to both brush and vF stimulation in *Tmem16f* cKO adapting neurons (unpaired mean difference brush: -11.4 [95% CI -19.2, -4.5], vF: -6.4 [95% CI -8.5, -4.5]) (Fig. 3c, d).

In summary, we report that dorsal horn microglia have a distinct phenotype during the first postnatal week characterized by high phagocytic activity, which coincides with postnatal engulfment of A-fibre terminals in the dorsal horn, supporting a role of microglia in developmental dorsal horn remodelling. We further show that disruption of microglial function by targeted deletion of *Tmem16f* during early postnatal life impairs microglia mediated A-fibre refinement in the dorsal horn leading to long-term changes in dorsal horn function and behaviour that persist into adulthood. Together, our data suggests that microglia mediated refinement of A-fibres during the early postnatal period is critical to both normal dorsal horn development and appropriate spatial encoding of dynamic touch.

The data here shows that most of the A-fibre engulfment occurs before P10 and decreases thereafter. Disrupting phagocytic capacity during this time by the conditional knockout of microglial *Tmem16f* increased the number of VGLUT1 presynaptic terminals in the superficial laminae, without altering the density of VGAT presynaptic terminals. This suggests that *Tmem16f* function is necessary for microglia mediated refinement of A-fibres and that this refinement is synapse specific.

Consistent with the increase in dorsal horn VGLUT1, *Tmem16f* cKO mice had enlarged brush receptive field areas in adapting (excitatory) neurons, which mirrors the large receptive field sizes in immature neonatal animals [13]. During the neonatal period A-fibre inputs dominate the superficial dorsal horn [14,15], and hindpaw receptive

fields are initially large, reducing in size over the first two postnatal weeks [13]. Functionally, this results in lower cutaneous mechanical thresholds, which together with immature local and descending inhibition leads to exaggerated reflex behaviour in neonates [1,7,13,16]. Both enlarged receptive field sizes and hypersensitivity were observed in *Tmem16f* cKO animals. This is unlikely due to local disinhibition [17,18], as spontaneous (Fig. S3b) and evoked activity of adapting WDR neurons were not increased, suggesting that the larger receptive field areas reflect a lack of primary afferent refinement, which leads to an increased spatial summation of dynamic inputs, and so an increased behavioural sensitivity to dynamic touch in *Tmem16f* cKO animals. The reduced firing rate of WDR neurons in response to dynamic touch may also be the result of the greater spread of A-fibre terminals in the dorsal horn. A potential mechanism underlying this effect is homeostatic synaptic downscaling, maintaining homeostasis by reducing neuronal firing rate when the overall network activity is increased [19].

Previous studies had shown that A-fibre refinement during postnatal development is activity dependent [3,4], but the exact mechanisms were unknown. Here we show that microglia mediate the physical removal of superfluous A-fibres in the dorsal horn and their function is necessary for normal dorsal horn circuit maturation. Preventing this process results in the persistence of enlarged touch receptive fields and hypersensitivity to dynamic touch into adulthood.

Materials and Methods

Animals

Sprague Dawley rats of both sexes were used for experiments in Fig. 1c-e and S1-2. Transgenic mice on C57BL/6J background of both sexes were used in all other experiments.

Experiments used the following transgenic mouse lines:

1. Ai9 / Rosa26-CAG::loxP-STOP-loxP-tdTomato-WPRE (Jackson Laboratory stock 007909 & 007905)

2. *Slc17a7*-IRES2-Cre (Jackson Laboratory stock 023527)

3. *Cx3cr1*-CreERT2-YFP (Jackson Laboratory stock 021160)

4. *Thy1*-EGFP-M (Jackson Laboratory stock 007788)

5. *Tmem16f*-floxed (flx) animals (Batti et al., 2016)

For visualisation of A-fibres, *Slc17a7*-IRES2-Cre (*Vglut1*-Cre) males (JAX stock no. 023527) were crossed with Ai9 females (JAX stock no. 007909) to obtain animals that expressed the tdTomato fluorophore under the *Vglut1* promoter ($Vglut1^{Cre/+}$:: $R26^{LSL\text{-}Ai9/+}$).

To generate tamoxifen inducible microglia-specific *Tmem16f* knock-out mice (*Tmem16f* cKO), Cx3cr1-CreER-YFP (JAX stock no. 021160) mice were crossed to *Tmem16f*-flx animals (generated by P. Heppenstall, see Batti et al. 2016), as well as Ai9 (JAX stock no. 007905) and *Thy1*-EGFP-M (JAX stock no. 007788).

Experimental animals were heterozygous for *Cx3cr1*-CreER-YFP ($^{CreER/+}$), homozygous for mutant conditional allele *Tmem16f*-flx ($^{fl/fl}$), and carrying Ai9 ($R26^{LSL\text{-}}$

^{Ai9}) and *Thy1*-eGFP (^{eGFP}) alleles (zygocity was not determined for $R26^{LSL\text{-}Ai9}$ and $Thy1^{eGFP}$). This produced the following genotype: $Cx3cr1^{CreER/+}$::$Tmem16f^{fl/fl}$::$R26^{LSL\text{-}Ai9}$::$Thy1^{eGFP}$. Control animals were homozygous for the wild type *Tmem16f* allele: $Cx3cr1^{CreER/+}$::$Tmem16f^{+/+}$::$R26^{LSL\text{-}Ai9}$::$Thy1^{eGFP}$.

Both females and males were used. No sex differences were expected and animals of both sexes were pooled together for analysis, but data points are presented as black (female) or red/magenta (male) to indicate the sexes. Numbers of animals used for each experiment are indicated in the figures. For a table with detailed species, ages, sexes, and numbers of animals used in each experiment, please see supplementary Table 1. All procedures were carried out in accordance with the guidelines of the UK Animals (Scientific Procedures) Act 1986 and subsequent amendments.

Drugs

4-hydroxytamoxifen (4-HT) was dissolved at 1mg/ml in corn oil, and 50µl was injected intragastrically per pup daily on three consecutive days from P1-3, following a previously described protocol [20]. Both control and experimental animals ($Tmem16^{+/+}$ and $Tmem16f^{fl/fl}$ respectively, see animals section above) received 4-HT injections to control for any effects of 4-HT itself. The dam was given a protein enriched diet a few days before and following delivery to aid milk production and pup survival.

Immunohistochemistry

Animals were overdosed with pentobarbital and transcardially perfused with saline followed by ice-cold 10% formalin. The sciatic nerve was exposed and traced to locate L4 & L5 dorsal root ganglia (DRG) and the corresponding region of the lumbar spinal

cord was dissected and post-fixed in 10% formalin overnight, followed by immersion in 30% sucrose until they sank. 50µm free-floating spinal cord sections were cut on the microtome with every 2nd section collected.

Tissue sections were washed 3 × 10 min in PBS and then incubated in blocking solution (10% donkey serum, 0.2% Triton X-100 in PBS) for 2.5h at room temperature. The sections were then incubated with primary antibodies at 4°C overnight followed by secondary antibodies at room temperature for 2h, both diluted in blocking solution (3% donkey serum, 0.2% Triton X-100 in PBS) (for list of antibodies and their respective concentrations used, see supplementary Table 2). Samples were mounted in Fluoromount Aqueous Mounting Medium (Sigma) or ProLong™ Diamond Antifade Mountant (Thermo Fischer), if the tissue contained endogenous fluorophores.

Behaviour

Behavioural testing was carried out on adult mice of both sexes between 3-4 months old, with the experimenter blinded to animal genotype/treatment. Animals were placed on a mesh platform (Ugo Basile) within individual transparent plastic chambers (6cm x 6cm x 12cm) for sensory testing of the plantar surface of the hind paw. Habituation and testing happened over five consecutive days. Animals were habituated to the testing environment for 1h per day on the first two days within individual plexicon chambers on the mesh platform. On the remaining days, animals were habituated for 30 min before being tested on each day. Brush response and von-Frey (vF) threshold were determined on the 3rd day, while repeated vF response testing was spread over the remaining 2 days to avoid sensitisation. Number of withdrawal reflexes were scored in each case, where only a rapid paw lifting was scored as a reflex. Animals

were allowed to rest at least 20 seconds between each stimulus. For brush response, a fine brush (Pro Arte, series 007, size 2) was moved over the plantar surface of the hind paw from heel to toe over a 2 second period [21]. This was repeated five times and the number of withdrawal reflexes out of five was recorded. vF threshold was assessed using the simplified up and down method [22]. Filaments were aimed at the region between the foot pads. Force was applied until the filament bent, and held in place for 2 seconds.

To generate a response curve to vF stimulation, repeated vF response was recorded by applying each of filaments no. 3 - 7 (0.04g - 0.6g) five times on the plantar surface, directed at the region between the foot pads. The sequence of vF filaments was randomised. Number of withdrawal reflexes out of five times was recorded.

In vivo extracellular recording

Animals subjected to behavioural testing were reused in electrophysiological recordings. Experimenter was blinded to animal genotype/treatment. All recordings were performed on adult mice (3-4 months old) of both sexes in the deep dorsal horn. Cells were not recorded beyond 550 µm depth from the surface of the spinal cord (see Fig. S2 for depth of all recorded neurons). 3-5 mice were used per sex and treatment group.

Animal preparation

Mice were anaesthetised with intraperitoneal urethane injection (10% in saline, 1.5g/kg). 100µl of 0.6 g/ml atropine and 200µl saline were injected subcutaneously to respectively counteract the mucus-driving side effect of urethane and to prevent

dehydration. The animal was constantly monitored for depth of anaesthesia throughout the experiment and supplemented with 50µl (5µg) urethane as needed. 200µl of saline was supplemented every 2 hours. Body temperature of the animal was kept close to 37°C with a heating pad throughout.

After cessation of reflexes, a tracheotomy was performed and a short plastic tube of about 1cm inserted to aid free breathing of the animal. The animal was then transferred onto a stereotactic frame and fixed with ear and hip bars. A laminectomy was carried out at vertebral level T13-L1 which corresponds to the spinal segments L4-L5 underneath. The spinal column was clamped for stability, the dura was removed, and the exposed spinal cord was covered with mineral oil to prevent drying.

Single unit extracellular recordings

A carbon micro-electrode (Carbostar-1, Kation Scientific) was lowered with a motorised manipulator (Scientifica) into the exposed spinal cord at a constant speed. A reference electrode was inserted into the back muscle close to the laminectomy for differential recording. Recorded neural activity was amplified 2000 times, and filtered for signals between 1kHz-10kHz (NL104 amplifier and NL125/6 band-pass filter modules from NeuroLog Digitimer). The signal was sampled at 20kHz and digitised using Powerlab 4/30 (ADInstruments). The trace was recorded and analysed in the software LabChart 7 (ADInstruments).

To isolate single neurons, the plantar surface of the animal's hind paw was gently continuously stroked as a searching signal, while the electrode is being lowered through the dorsal horn of the spinal cord. Once a cell has been identified by equal amplitude of the spikes recorded, the brush receptive field of the cell was mapped out

by a fine brush (Pro Arte, series 202, size 1, brush tip cut short to 7mm length x 1mm width).

Spontaneous activity was recorded for 10 min before and 5 min after stimulation. To record brush and von-Frey (vF) fibre evoked activity from single neurons, each stimulus was applied for 2 seconds over the receptive field of the cell and repeated 3 times, with a minimum of 10 second interval in between.

Cells were not recorded if they exhibited very high spontaneous firing rates that did not allow evoked activity to be clearly distinguished from spontaneous activity. Only wide dynamic range neurons responding both to brush and pinch stimulation were recorded. Animals were euthanised at the end of the experiment and the spinal cord was collected in neutral buffered 10% formalin (overnight) followed by 30% sucrose solution for re-use in immunohistochemistry.

Analysis & cell type categorisation

Analysis was carried out in the LabChart 7 software (ADInstruments). For spontaneous activity, firing rate was analysed over a 10min window prior to applying any stimuli. Firing rate for evoked responses were analysed over the first second of the stimulus duration and averaged over three trials.

Cells were divided into adapting and non-adapting groups based on their firing properties towards a threshold vF-stimulus [12]. This threshold vF was defined as the first vF filament that evokes a firing rate of 10Hz or more. The response within the first second of vF application was

analysed to calculate an adaptive ratio R, which was defined as

$$R = \frac{Number\ of\ spikes\ fired\ between\ 0.5 - 1\ sec}{Number\ of\ spikes\ fired\ between\ 0 - 0.5\ sec}$$

If a cell adapts rapidly to stimulation, one would expect R to be close to zero, as barely any spikes should be fired between 0.5 - 1 sec, however, if a cell is non-adapting and firing continuously, one would expect R to be close to 1. To decide the boundary between adapting and non-adapting cells we used k-means cluster analysis, which sorted the values into two groups that is equivalent to a boundary at R = 0.33. For the k-means clustering we included cells from a previous experiment.

Image acquisition and analysis

Confocal z-stacks were taken with a Zeiss LSM880 confocal microscope or Yokogawa CSU22 spinning disk microscope using a 20× water immersion objective (NA 1.0) for imaging of A-fibres and 63× oil immersion objective (NA 1.4) followed by analysis in Fiji software. Details on microscope settings can be found in supplementary Table 1 and in the metadata of example images online at https://github.com/Yajing826/A-fibre-engulfment. Only intact sections with an even stain were analysed, and at least 6 sections were imaged and analysed per animal to reduce variability.

Cell counts and phagocytic cup counts were performed manually on confocal images in Volocity, with the experimenter blinded to the age groups. Phagocytic cups were defined as any rounded structure at the end of a microglial process. CD68-high microglia cells were defined as any Iba1 positive cell that contains at least two CD68 puncta.

A-fibre engulfment by microglia and synapse density were analysed with automated batch processing in Fiji using the 3D-ROI manager plugin and custom written macros

[23–26]. For A-fibre engulfment, each of the channels containing staining for microglia/lysosomes/A- fibres were binarized and the volume of their overlap measured. For synapse density measures, the channel containing synaptic stain was binarized and segmented, following which volume and object numbers were recorded. Macro scripts for the automated analysis are available online at https://github.com/Yajing826/A-fibre-engulfment.

Statistical Analysis

Estimation statistics for the 95% confidence intervals (95% CI) of the mean difference were calculated on estimationstats.com [27] using 5000 samples of bias-corrected and accelerated bootstrapping. As bootstrapping is less accurate for small samples sizes [28], confidence intervals were only calculated for samples with N≥5. For Fig. 1d, e, and S1, S2 where N=4, one-way ANOVA was used with post-hoc comparisons carried out using Dunnett's method.

Additionally, conventional null-hypothesis significance testing were carried out on estimationstats.com and GraphPad Prism 6 for all comparisons (significance level was set at $\alpha=0.05$), which are listed in the supplementary Table 1.

Data are presented as mean ± SD in all figures. Where applicable, the effect size is presented as 95% CI of the mean difference on a separate but aligned axis. The mean difference is plotted as a dot on the background of its probability distribution, and the 95% confidence interval is indicated by the ends of the error bar. All values in text and figures are given with two decimals or rounded to two significant figures. N-numbers are as indicated in figures. For a comprehensive list with exact statistical values and analyses, see supplementary Table 1.

Acknowledgements

This work was supported by the NIAA (SB), Wellcome Trust (YX)

Author Contributions

YX, SK, MF and SB designed the study, performed the experiments, analysed and interpreted data and co-wrote the manuscript. AC, QH and RRJ developed the mouse model and prepared tissue for analysis. MS and PH developed the mouse model. RRJ, PH and other co-authors edited the manuscript.

Competing Interest Statement

The authors declare no competing interests.

References

1. Koch, S. C. & Fitzgerald, M. Activity-dependent development of tactile and nociceptive spinal cord circuits. *Ann. N. Y. Acad. Sci.* **1279**, 97–102 (2013).
2. Schouenborg, J. Action-based sensory encoding in spinal sensorimotor circuits. *Brain Res. Rev.* **57**, 111–117 (2008).
3. Beggs, S., Torsney, C., Drew, L. J. & Fitzgerald, M. The postnatal reorganization of primary afferent input and dorsal horn cell receptive fields in the rat spinal cord is an activity-dependent process. *Eur. J. Neurosci.* **16**, 1249–1258 (2002).
4. Granmo, M., Petersson, P. & Schouenborg, J. Action-Based Body Maps in the Spinal Cord Emerge from a Transitory Floating Organization. *J. Neurosci.* **28**, 5494–5503 (2008).
5. Fitzgerald, M. & Jennings, E. The postnatal development of spinal sensory processing. *Proc. Natl. Acad. Sci. U. S. A.* **96**, 7719–7722 (1999).
6. Jennings, E. & Fitzgerald, M. C-fos can be induced in the neonatal rat spinal cord by both noxious and innocuous peripheral stimulation. *Pain* **68**, 301–306 (1996).
7. Fitzgerald, M., Shaw, A. & MacIntosh, N. Postnatal development of the

cutaneous flexor reflex: comparative study of preterm infants and newborn rat pups. *Dev. Med. Child Neurol.* **30**, 520–526 (1988).

8. Salter, M. W. & Stevens, B. Microglia emerge as central players in brain disease. *Nat. Med.* **23**, 1018–1027 (2017).
9. Chamessian, A. *et al.* Is Optogenetic Activation of Vglut1-Positive Aβ Low-Threshold Mechanoreceptors Sufficient to Induce Tactile Allodynia in Mice after Nerve Injury? *J. Neurosci.* **39**, 6202–6215 (2019).
10. Batti, L. *et al.* TMEM16F Regulates Spinal Microglial Function in Neuropathic Pain States. *Cell Rep.* **15**, 2608–2615 (2016).
11. Taylor-Clark, T. E. *et al.* Thy1.2 YFP-16 Transgenic Mouse Labels a Subset of Large-Diameter Sensory Neurons that Lack TRPV1 Expression. *PLoS One* **10**, e0119538 (2015).
12. Lee, K. Y., Ratté, S. & Prescott, S. A. Excitatory neurons are more disinhibited than inhibitory neurons by chloride dysregulation in the spinal dorsal horn. *Elife* **8**, (2019).
13. Fitzgerald, M. The post-natal development of cutaneous afferent fibre input and receptive field organization in the rat dorsal horn. *J. Physiol.* **364**, 1–18 (1985).
14. Baccei, M. L., Bardoni, R. & Fitzgerald, M. Development of nociceptive synaptic inputs to the neonatal rat dorsal horn: Glutamate release by capsaicin and menthol. *J. Physiol.* **549**, 231–242 (2003).
15. Fitzgerald, M. & Gibson, S. The postnatal physiological and neurochemical development of peripheral sensory C fibres. *Neuroscience* **13**, 933–944 (1984).
16. Fitzgerald, M. What do we really know about newborn infant pain? *Exp.*

Physiol. **100**, 1451–1457 (2015).

17. Takeda, M., Tanimoto, T. & Matsumoto, S. Change in mechanical receptive field properties induced by GABA(A) receptor activation in the trigeminal spinal nucleus caudalis neurons in rats. *Exp. Brain Res.* **134**, 409–416 (2000).
18. Zieglgänsberger, W. & Herz, A. Changes of cutaneous receptive fields of spino-cervical-tract neurones and other dorsal horn neurones by microelectrophoretically administered amino acids. *Exp. Brain Res.* **13**, 111–126 (1971).
19. Siddoway, B., Hou, H. & Xia, H. Molecular mechanisms of homeostatic synaptic downscaling. *Neuropharmacology* **78**, 38–44 (2014).
20. Pitulescu, M. E., Schmidt, I., Benedito, R. & Adams, R. H. Inducible gene targeting in the neonatal vasculature and analysis of retinal angiogenesis in mice. *Nature Protocols* vol. 5 1518–1534 (2010).
21. Duan, B. *et al.* Identification of spinal circuits transmitting and gating mechanical pain. *Cell* **159**, 1417–1432 (2014).
22. Bonin, R. P., Bories, C. & De Koninck, Y. A Simplified Up-Down Method (SUDO) for Measuring Mechanical Nociception in Rodents Using von Frey Filaments. *Mol. Pain* **10**, 1744-8069-10–26 (2014).
23. Ollion, J., Cochennec, J., Loll, F., Escudé, C. & Boudier, T. TANGO: a generic tool for high-throughput 3D image analysis for studying nuclear organization. *Bioinformatics* **29**, 1840–1841 (2013).
24. Linkert, M. *et al.* Metadata matters: access to image data in the real world. *J. Cell Biol.* **189**, 777–782 (2010).
25. Schindelin, J. *et al.* Fiji: an open-source platform for biological-image analysis. *Nat. Methods* **9**, 676–682 (2012).

26. Schneider, C. A., Rasband, W. S. & Eliceiri, K. W. NIH Image to ImageJ: 25 years of image analysis. *Nat. Methods* **9**, 671–675 (2012).

27. Ho, J., Tumkaya, T., Aryal, S., Choi, H. & Claridge-Chang, A. Moving beyond P values: data analysis with estimation graphics. *Nat. Methods* **16**, 565–566 (2019).

28. Chernick, M. R. *Bootstrap Methods*. (John Wiley & Sons, Inc., 2007). doi:10.1002/9780470192573.